Theor Chem Acc (2012) 131:1248
DOI 10.1007/s00214-012-1248-1

REGULAR ARTICLE

Spin trapping of hydroperoxyl radical by a cyclic nitrone conjugated to β-cyclodextrin: a computational study

Xiaoguang Bao · Peng Tao · Frederick A. Villamena · Christopher M. Hadad

Received: 29 December 2011 / Accepted: 19 June 2012 / Published online: 17 July 2012

Abstract Spin trapping of hydroperoxyl radical ($HOO^{\cdot}$) by the amide-linked conjugate of 5-carbamoyl-5-methyl-1-pyrroline *N*-oxide (AMPO) to β-cyclodextrin (β-CD) was studied computationally using a two-layered ONIOM method. From a conformational perspective, the "internal" conformation of 5*R*-β-CD-AMPO is more favored than the "external" conformation in which the nitrone is located outside of the cavity of the β-CD. When the $HOO^{\cdot}$ addition product is formed, the most stable isomer has the nitroxyl (N_1–O_1) moiety pointing inside the cavity of the β-CD. Thus, this "internal" conformation might protect the N_1–O_1 moiety of the resulting spin adduct from access by reducing agents, thereby improving the lifetime of the radical adduct. The computed energetic barrier for $HOO^{\cdot}$ addition to the 5*R*-β-CD-AMPO is 8.7 kcal/mol, which is marginally smaller than spin trapping by the non-conjugated AMPO (that is, without the β-CD). To optimize the reactivity of the β-CD-AMPO conjugate, the effect of a spacer unit between the AMPO segment and the β-CD moiety with varying methylene units, $(CH_2)_n$ ($n = 1, 2, 3$), on the energetics of $HOO^{\cdot}$ addition was evaluated. The structure with only one methylene spacer ($n = 1$) appears to be optimal as determined by the smaller activation barrier (6.2 kcal/mol) for $HOO^{\cdot}$ addition to the nitrone moiety. Compared with very time-consuming quantum mechanical methods, the ONIOM method appears to offer significant advantages for evaluation of the best β-CD-AMPO conjugate for trapping of such reactive oxygen species and providing for the rational design of novel nitrones as spin traps.

Keywords Nitrone · Spin trapping · Hydroperoxyl radical · Electron paramagnetic resonance spectroscopy · Cyclodextrin

1 Introduction

It is well accepted that overproduction of reactive oxygen-centered radicals is associated with the pathogenesis of many human diseases [1–3]. In situations of oxidative stress, superoxide radical anion ($O_2^{\cdot-}$) is often initially formed and can then facilitate the formation of other reactive oxygen species (ROS). The protonated form of $O_2^{\cdot-}$, hydroperoxyl radical ($HOO^{\cdot}$), has also received much attention due to its high reactivity and its uncharged nature, which might allow it to cross membranes more readily than the charged $O_2^{\cdot-}$; [4] however, hydroperoxyl radical is two or three orders of magnitude lower in concentration than $O_2^{\cdot-}$ at physiological pH [5]. Spin trapping using nitrones (e.g., 5,5-dimethyl-1-pyrroline *N*-oxide (DMPO) [6–10] or α-phenyl-*N*-tert-butylnitrone (PBN) [11, 12]) in combination with electron paramagnetic resonance (EPR) spectroscopy [10] has been a popular technique for the detection of oxygen-centered radicals (Scheme 1).

Electronic supplementary material The online version of this article (doi:10.1007/s00214-012-1248-1) contains supplementary material, which is available to authorized users.

X. Bao · C. M. Hadad (✉)
Department of Chemistry, Ohio State University,
100 West 18th Avenue, Columbus, OH 43210, USA
e-mail: hadad.1@osu.edu

P. Tao
Department of Chemistry, Wayne State University,
5101 Cass Avenue, Detroit, MI 48202, USA

F. A. Villamena
Department of Pharmacology, Davis Heart and Lung Research Institute, Ohio State University, Columbus, OH 43210, USA

Scheme 1 DMPO, AMPO and PBN

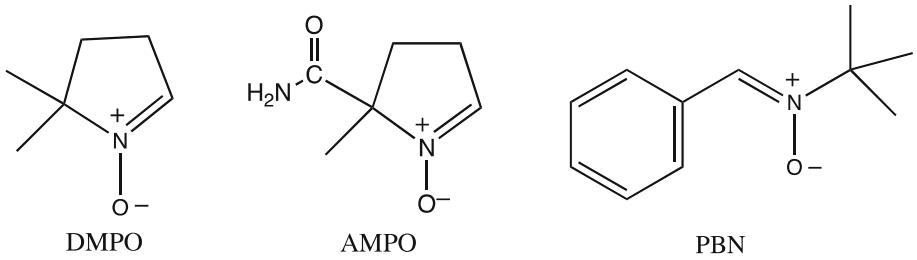

However, the use of these spin traps has limitations; [13–15] for instance, the lifetime of the generated radical adducts is relatively short in the case of the $O_2^{\cdot-}$ adduct or the species are redox active.

The development of spin-trapping agents with more improved properties is ongoing, especially for more efficient radical trapping and improvement in the stability of the resulting spin adducts. During the past several decades, various derivatives of DMPO and other nitrones were synthesized and investigated, many with improved spin-trapping properties [16–27]. Ligation of the trapping agents to some carriers could provide solutions for the detection of radicals at the site of their production in cellular systems [28, 29]. However, the presence of highly reducing species, such as ascorbate, thiols, or metal ions, in cellular systems can significantly reduce the lifetime of the spin adducts. Exposure of the N–O moiety of the spin adduct to the reducing environment was hypothesized to be responsible for their bioreducibility [33]. We posit that protection of the N–O moiety of the nitrones and the spin adducts from reducing species might provide improved spin trap bioavailability and increased lifetime of the spin adducts.

One way to protect the radical spin adduct from reduction might be to sequester the product within a hydrophobic cavity. Cyclodextrins, which are composed of carbohydrates, have hydrophobic interiors but have secondary hydroxyl groups that line the top and bottom rims. Bardelang et al. [30] recently demonstrated that the half-life of the free PBN–$HOO^{\cdot}$ adduct can indeed be increased to 3 min even in the presence of sodium L-ascorbate through inclusion with β-cyclodextrin (β-CD). However, the relatively high concentration of β-CD might limit the application of this spin-trapping method in vivo. To improve the performance of this method, PBN was ligated to β-CD and shown to have very promising properties for the persistence of the corresponding radical adducts [31, 32]. Moreover, the synthesis of 5-carbamoyl-5-methyl-1-pyrroline *N*-oxide (AMPO) covalently linked to β-CD has been reported, and this conjugate was shown to improve spin-trapping performance and spin-adduct stability [33]. The maximum half-life of $t_{1/2} = 27.5$ min at pH 7.0 was achieved for $O_2^{\cdot-}$ trapping by this β-CD-AMPO conjugate [33]. The presence of intramolecular H-bonding interactions might also play a significant role in facilitating $HOO^{\cdot}$ addition to nitrones [34].

Understanding the various modes of interaction from a theoretical point of view would be helpful in order to design better spin traps based on the conjugation of nitrones to β-CD. Although some very low-level molecular modeling approaches have been employed to study the β-CD-AMPO conjugate [33], any intramolecular H-bonding interactions between grafted AMPO and β-CD were not revealed. The effect of the length of the linker between AMPO and the β-CD on the spin-trapping properties is of interest. Moreover, theoretical details on the kinetics of trapping of $HOO^{\cdot}$ or $O_2^{\cdot-}$ by β-CD-AMPO are still lacking [33]. For a number of years, we have demonstrated success in the use of theoretical methods for the rational design of nitrones as EPR spin traps as well as in the determination of the kinetic parameters for spin trapping [34–40].

In this work, spin trapping of $HOO^{\cdot}$ by the amide-linked conjugate of AMPO to β-CD was studied using a two-layered ONIOM method and compared with a complete quantum mechanical (QM) method. To optimize the reactivity of the β-CD-AMPO conjugate, a spacer unit with varying methylene units, $(CH_2)_n$ ($n = 1, 2, 3$), was evaluated between the AMPO segment and the β-CD moiety. These computational studies were used to aid the rational design of more efficient spin traps for reactive oxygen species.

2 Computational methods

Calculations of the β-CD-AMPO and its corresponding $HOO^{\cdot}$ spin adducts were performed using the two-layered ONIOM method [41, 42] as implemented in the Gaussian 03 program [43]. The ONIOM method is a multilevel, subtractive QM/MM extrapolation method in which the studied molecular system is divided into two or more parts or layers. The most important layer from a chemical point of view is treated at a high level of ab initio molecular orbital method, and the rest of the system is described by a computationally less demanding method (such as the lowest ab initio approximation or semiempirical or molecular mechanics approximations). In the current effort, the β-CD-AMPO model was divided into two layers.

The high layer, using the B3LYP/6-31G(d) method [44, 45], includes the AMPO and the upper CH_2OH groups of β-CD (shown in Fig. 1). The other atoms of β-CD, belonging to the low layer, were treated using the PM3 semi-empirical method [46], which has been shown to give very reasonable geometrical parameters for cyclodextrins [47]. The two layers are connected by link atoms. The molecule β-CD-AMPO and the $HOO^{\cdot}$ adduct were also fully optimized at the B3LYP/6-31G(d) level of theory, and single-point energies were then computed at the B3LYP/6-31+G(d,p)//B3LYP/6-31G(d) level of theory to evaluate the performance of the ONIOM method. Such single-point calculations with the B3LYP functional have been successfully applied to conformational issues with carbohydrates [48]. A variety of conformations were examined, varying in their orientation of hydrogen bonds.

To predict the energy barrier for the trapping of $HOO^{\cdot}$ by β-CD-AMPO, potential energy surface (PES) scans along the C_2–O_b bond cleavage of β-CD-AMPO-$HOO^{\cdot}$ were investigated using the two-layered ONIOM method. The C_2–O_b bond length (R) was stretched in units of 0.05 Å, from 1.40 to 3.40 Å. At each value of R, the other coordinates of the complex were fully optimized. The PES near to the peak was then scanned in smaller steps of 0.01 Å to obtain a more accurate structure and energy of the transition state. The products and initial reactants were fully optimized to local minima using the same ONIOM method. Single-point energies on the optimized ONIOM(B3LYP/6-31G(d):PM3) geometries were calculated at ONIOM(B3LYP/6-31+G(d,p):PM3) level of theory. To understand whether the PES scan could give a reasonable transition state structure and energy barrier using ONIOM method, fully optimized QM studies at the B3LYP/6-31G(d) level of theory were performed. The molecules with varying spacer units, $(CH_2)_n$ ($n = 1, 2, 3$), between the AMPO segment and the β-CD moiety were evaluated with the same strategy (Scheme 2).

For comparison, the spin trapping of $HOO^{\cdot}$ by AMPO was studied at the B3LYP/6-31G(d) level of theory. The non-conjugated AMPO nitrone with $HOO^{\cdot}$ complex and spin-adduct structures were fully optimized to local minima, and each stationary point was determined to have zero imaginary vibrational frequencies. Transition states for the trapping of $HOO^{\cdot}$ were characterized as having only one imaginary vibrational frequency. The corresponding normal mode for the imaginary vibrational frequency then suggested the related reactant and product for that transition state. Single-point energies on the optimized B3LYP/6-31G(d) geometries were evaluated at the B3LYP/6-31+G(d,p) level of theory. The bottom-of-the-well energy will be used for the following discussion.

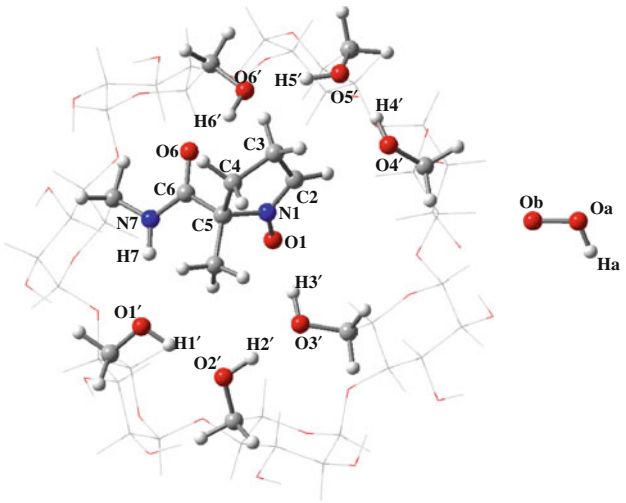

Fig. 1 Two partition schemes used for the two-layer ONIOM calculation of the β-CD-AMPO. The high layer (B3LYP/6-31G(d)) is noted with a *ball* and *stick* model. The low layer (PM3) is represented as a *line* model. The atomic numbering is also provided and used in the discussion

3 Results and discussion

3.1 "Internal" and "external" conformations of the β-CD-AMPO conjugates

The cyclic nitrone, when grafted to the narrow rim of the β-CD by an amide bond linkage, functions like a lid, which may be "open" or "closed" relative to the rest of the cyclodextrin. Two typical isomers were explored, which represented the "open" and "closed" conformation of β-CD-AMPO at the ONIOM(B3LYP/6-31G(d):PM3) level. Both of the stereoisomeric structures (5*R* and 5*S*) of β-CD-AMPO were considered. To evaluate the performance of the ONIOM method, additional (and very time-consuming) optimizations of the β-CD-AMPO conjugate were also

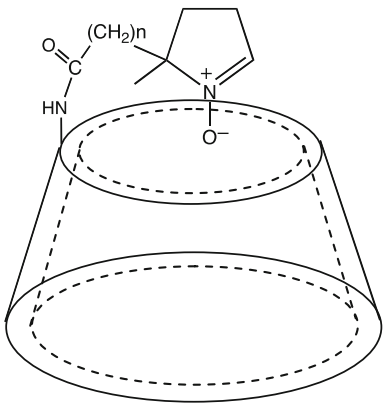

Scheme 2 β-CD-A-$(CH_2)_n$-MPO ($n = 1, 2, 3$). For clarity, the β-CD is shown as a truncated barrel

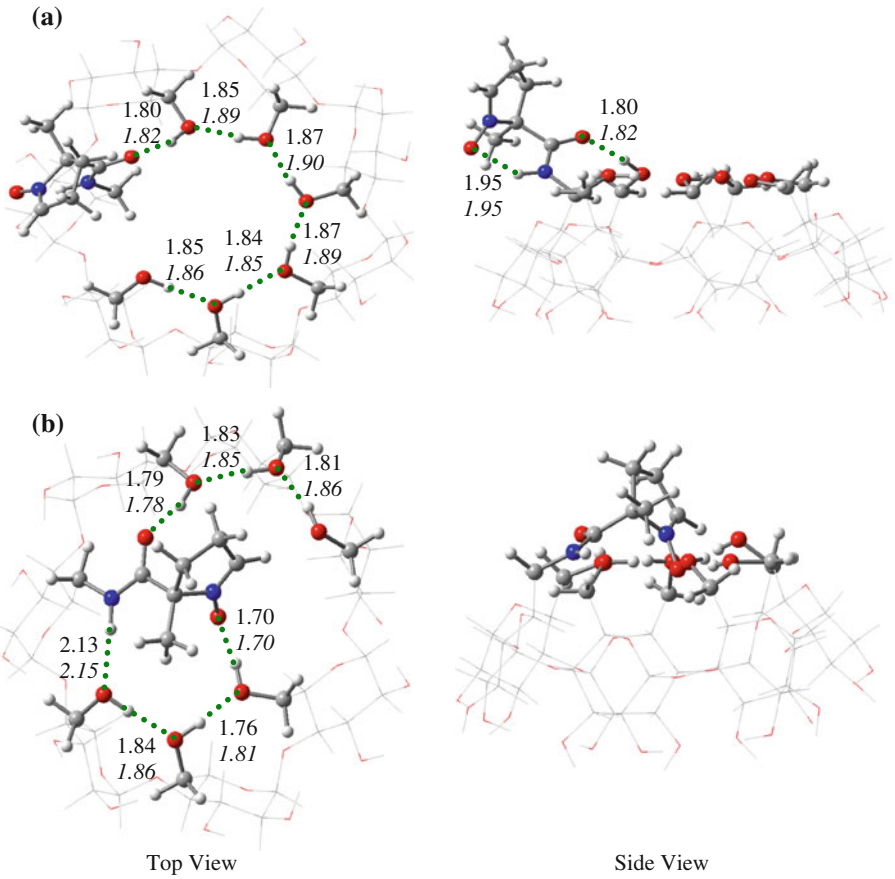

Fig. 2 Two views of the optimized structure of **a** "external" and **b** "internal" conformations of 5*R*-*β*-CD-AMPO as calculated with the ONIOM(B3LYP/6-31G(d):PM3) method. The H-bond lengths are shown in normal text. The H-bond lengths obtained from the QM optimized structure of *β*-CD-AMPO are listed in italics for comparison. The *colors* represent the following atoms: *gray* is for carbon, *white* is for hydrogen, *red* is for oxygen, and *blue* is for nitrogen. Bond lengths are shown in angstroms (Å)

carried out at the B3LYP/6-31G(d) level of theory to provide calibration of this approach.

The optimized structure of the "external" conformation of 5*R*-*β*-CD-AMPO at the ONIOM(B3LYP/6-31G(d):PM3) level of theory is shown in Fig. 2a (top and side views are provided). The primary hydroxyl groups crowning the narrower rim form a half-circle as a H-bond chain. The H-bond lengths vary from 1.80 to 1.87 Å. This hydrogen-bonding mode is consistent with the favored structure of α-CD in the gas phase [49]. Moreover, the amide linkage also forms an intramolecular H-bond with the nitrone moiety (N_1–$O_{\dot{1}}\cdots H_7$–N_7). The five-membered ring of AMPO does not interact with any hydroxyl groups of *β*-CD in the "external" conformation. In comparison with the fully optimized structure at the B3LYP/6-31G(d) level of theory, the ONIOM method gives a very similar structure at relatively inexpensive cost.

As for the "internal" conformation of the 5*R*-*β*-CD-AMPO (Fig. 2b), a H-bond chain was also formed, bridged by the amide linker (1.79 Å for $O_{6'}H_{\ddot{6}'}\cdots O_6{=}C_6$ and 2.13 Å for $N_7H_{\ddot{7}}\cdots O_{1'}H_{1'}$) at the rim. Another striking feature for the "internal" conformation is the formation of N_1–$O_{\dot{1}}\cdots H_{3'}O_{3'}$ H-bond (1.70 Å) between the N_1–O_1 moiety of AMPO and the $H_{3'}O_{3'}$ groups of *β*-CD. This H-bond may play an important role in keeping the N_1–O_1 moiety of AMPO pointing into the cavity of *β*-CD. The H-bond length differences between the ONIOM method and QM method are less than 0.05 Å. It appears that the ONIOM method works well for the geometrical optimization of the *β*-CD-AMPO conjugate.

The "internal" and "external" isomers of 5*S*-*β*-CD-AMPO were also investigated (see supporting information, Figure S1). Little geometrical difference of the *β*-CD part was observed for the "external" isomer between the 5*R*- and 5*S*-*β*-CD-AMPO. As for the "internal" conformer of 5*S*-*β*-CD-AMPO, however, the H-bond chain showed differences in comparison with the 5*R*-*β*-CD-AMPO. The $O_{3'}H_{\ddot{3}'}\cdots O_{4'}H_{4'}$ H-bond was formed for 5*S*-*β*-CD-AMPO but was not observed for 5*R*-*β*-CD-AMPO. The $O_{4'}H_{\ddot{4}'}\cdots O_{5'}H_{5'}$ H-bond was not seen in the 5*S*-*β*-CD-AMPO, but it existed in the 5*R*-*β*-CD-AMPO. For the internal conformers, hydrogen-bonding patterns change (N_1–$O_{\dot{1}}\cdots H_{4'}O_{4'}$ for 5*S*-*β*-CD-AMPO and N_1–$O_{\dot{1}}\cdots H_{3'}O_{3'}$ for 5*R*-*β*-CD-AMPO), but the number of H-bond partners is conserved.

Table 1 gives the relative energies of these four conformers. The "internal"-5*R*-*β*-CD-AMPO isomer is 9.5 kcal/mol lower than the "external"-5*R*-*β*-CD-AMPO at the ONIOM(B3LYP/6-31+G(d,p):PM3)//ONIOM(B3LYP/6-31G(d):PM3) level of theory; thus, the "internal" conformation is much more favored for the *β*-CD-AMPO conjugate. Optimized structures

Table 1 Relative energies of the "internal" and "external" conformations of the 5*R*- and 5*S*-*β*-CD-AMPO conjugates (in kcal/mol)

	ONIOM(B3LYP/6-31G(d):PM3)	ONIOM(B3LYP/6-31+G(d,p):PM3)//ONIOM(B3LYP/6-31G(d):PM3)	B3LYP/6-31G(d)	B3LYP/6-31+G(d,p)//B3LYP/6-31G(d)
5*R*-"Internal"	0.0	0.0	0.0	0.0
5*R*-"External"	11.6	9.5	8.1	5.3
5*S*-"Internal"	3.3	3.4	4.7	4.5
5*S*-"External"	11.5	9.4	8.6	5.6

of these two isomers at the B3LYP/6-31G(d) level of theory give an 8.1 kcal/mol energy difference, and the single-point energy at the B3LYP/6-31+G(d,p)//B3LYP/6-31G(d) level reduces this preference to 5.3 kcal/mol. For each of these levels of theory, the "internal"-5*R*-*β*-CD-AMPO conformer is considerably more stable than the "external"-5*R*-*β*-CD-AMPO conformer.

However, the energy difference between the "internal" and "external" conformers of the 5*S* analog is much smaller. For 5*S*-*β*-CD-AMPO, the "internal" isomer is only 1.1 kcal/mol more stable than the "external" isomer at the B3LYP/6-31+G(d,p)//B3LYP/6-31G(d) level.

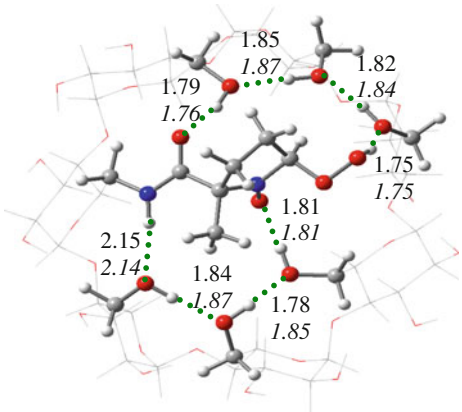

5R-β-CD-AMPO-HOO•-1

Fig. 3 The optimized 5*R*-*β*-CD-AMPO-HOO˙-1 isomer obtained at the ONIOM(B3LYP/6-31G(d):PM3) level of theory. The H-bond lengths are shown in normal text. The H-bond lengths obtained from the fully optimized B3LYP structure are given in *italics* for comparison. The *colors* represent the following atoms: *gray* is for carbon, *white* is for hydrogen, *red* is for oxygen, and *blue* is for nitrogen. Bond lengths are shown in angstroms (Å)

3.2 Conformations of the *β*-CD-AMPO-HOO˙ spin adducts

3.2.1 Geometries and relative energies

Since the HOO group can act as both a H-bond donor and acceptor when interacting with hydroxyl groups of *β*-CD, three different spin-adduct conformers (5*R*-*β*-CD-AMPO-HOO˙-1 to 5*R*-*β*-CD-AMPO-HOO˙-3) were studied on the basis of the most stable "internal" conformation of 5*R*-*β*-CD-AMPO. For the "external" conformation of 5*R*-*β*-CD-AMPO, spin-adduct 5*R*-*β*-CD-AMPO-HOO˙-4 was studied. Spin adducts 5*S*-*β*-CD-AMPO-HOO˙-1 and 5*S*-*β*-CD-AMPO-HOO˙-2 were also studied based on the "internal" and "external" conformers of the 5*S*-*β*-CD-AMPO, respectively. The optimized structure of 5*R*-*β*-CD-AMPO-HOO˙-1 is depicted in Fig. 3, and the others are shown in the supporting information (Figure S2). The relative energies of these conformers were listed in Table 2. To evaluate the performance of the ONIOM method on the radical adducts, full geometry optimizations of the *β*-CD-AMPO-HOO˙ adduct were carried out at the UB3LYP/6-31G(d) level of theory.

The 5*R*-*β*-CD-AMPO-HOO˙-1 isomer, in which the HOO group only acts as a H-bond donor ($HO_aO_b\cdots H_{4'}O_{4'}$) with the $H_{4'}O_{4'}$ group of *β*-CD, is the most stable conformer among these four spin-adduct product isomers (Table 2). The H-bond length ($H_aO_aO_b\cdots H_{4'}O_{4'}$) is only 1.75 Å. The other H-bond modes of this conformer change little

Table 2 Relative energies of four isomers of 5*R*-*β*-CD-AMPO-HOO˙ (in kcal/mol)

	ONIOM(B3LYP/6-31G(d):PM3)	ONIOM(B3LYP/6-31+G(d,p):PM3)//ONIOM(B3LYP/6-31G(d):PM3)	B3LYP/6-31G(d)	B3LYP/6-31+G(d,p)//B3LYP/6-31G(d)
5*R*-*β*-CD-AMPO-HOO˙-1	0.0	0.0	0.0	0.0
5*R*-*β*-CD-AMPO-HOO˙-2	9.0	7.8	8.6	7.8
5*R*-*β*-CD-AMPO-HOO˙-3	12.5	11.8	10.5	11.4
5*R*-*β*-CD-AMPO-HOO˙-4	12.4	9.5	8.6	4.8

compared with the intact "internal" 5*R*-*β*-CD-AMPO. Moreover, the difference of corresponding H-bond lengths between 5*R*-*β*-CD-AMPO-HOO˙-1 and "internal" 5*R*-*β*-CD-AMPO is no more than 0.02 Å except N_1–O_i···$H_{3'}O_{3'}$, which is 0.11 Å longer for the spin-adduct product. The N_1–O_i···$H_{3'}O_{3'}$ H-bond may stabilize the N_1–O_1 moiety of AMPO pointing into the cavity of *β*-CD. This conformation may protect the N_1–O_1 moiety of the spin-adduct product from access to reducing species, thereby perhaps increasing the lifetime of the spin-adduct product. The H-bond distances obtained by ONIOM and B3LYP methods are very similar except the $O_{2'}H_{2'}$···$O_{3'}H_{3'}$ (1.78 Å for ONIOM vs. 1.85 Å for B3LYP).

Although both 5*R*-*β*-CD-AMPO-HOO˙-2 and 5*R*-*β*-CD-AMPO-HOO˙-3 isomers form two H-bonds between the HOO group and the rim hydroxyl groups of *β*-CD (Figure S2), the relative energies of the two conformers are 7.8 and 11.8 kcal/mol, respectively, higher than the most stable one using ONIOM method (Table 2), indicating that these two isomers are not favorable structures. The relative (ONIOM) energy of the 5*R*-*β*-CD-AMPO-HOO˙-4 isomer, which is based on the "external" conformation of 5*R*-*β*-CD-AMPO, is 9.5 kcal/mol larger than the most stable 5*R*-*β*-CD-AMPO-HOO˙-1 isomer. The "external" spin-adduct structure is also not favorable relative to the "internal" conformation. Larger relative energy differences between ONIOM and B3LYP methods were found for this "external" HOO˙ adduct isomer in comparison with the "internal" HOO˙ adduct isomers.

In addition, the corresponding HOO˙ spin adducts 5*S*-*β*-CD-AMPO-HOO˙-1 and 5*S*-*β*-CD-AMPO-HOO˙-2 were investigated based on the "internal" and "external" conformers of the 5*S*-*β*-CD-AMPO, respectively (supporting information, Figure S3). Although the topology of the H-bonds is quite different between these two isomers, the total number of H-bonds (8) is conserved. A striking feature on the relative energies (Table 3) is that only small energy differences between the 5*S*-*β*-CD-AMPO-HOO˙-1 and 5*S*-*β*-CD-AMPO-HOO˙-2 were noted according to the B3LYP results, and interestingly the ONIOM results suggest larger energy differences. The "internal" structure in which the N_1–O_1 moiety of the spin adduct is H-bonded to a hydroxyl group of *β*-CD may not play a significant role in the spin-trapping products by 5*S*-*β*-CD-AMPO. In comparison, the most stable "internal" isomer for the N_1–O_1 moiety being protected inside the cavity of the *β*-CD is the 5*R*-*β*-CD-AMPO-HOO˙ adduct. This observation may be an explanation accounting for the shorter half-life of the spin adduct derived from 5*S*-*β*-CD-AMPO [33].

3.2.2 *Potential energy surface for HOO˙ trapping*

On the basis of the most stable 5*R*-*β*-CD-AMPO-HOO˙-1 isomer, the C_2–O_b bond was stretched to investigate the ONIOM potential energy surface for the process of kinetic trapping of HOO˙ by *β*-CD-AMPO. Figure 4 shows that the peak of the PES was achieved when the C_2···O_b distance equals 2.06 Å. The PES becomes much flatter when the C_2···O_b distance reaches more than 3.30 Å where it seems a local minimum is reached. On the basis of these PES results, the initial complex of HOO˙ with *β*-CD-AMPO was fully optimized (Fig. 6). The distance between O_b of HOO˙ and C_2 of the nitrone is 3.47 Å. Based on the peak of PES and the starting complex of HOO˙ with *β*-CD-AMPO, the predicted energy barrier for trapping HOO˙ by *β*-CD-AMPO is 8.7 kcal/mol at the ONIOM(B3LYP/6-31+G(d,p):PM3)//ONIOM(B3LYP/6-31G(d):PM3) level of theory. The product energy is 12.4 kcal/mol lower than the initial complex (Table 4).

In order to ascertain whether the potential energy surface study could give a reasonable structure of the transition state (TS) of HOO˙ addition, the TS structures for HOO˙ addition have been located at the B3LYP/6-31G(d) level of theory. The C_2···O_b distance is 2.06 Å similar to the ONIOM PES (Figs. 5, 6). Moreover, the H-bond lengths show little difference. The PES scan for HOO˙ addition using the ONIOM method provides a very good TS structure for this radical addition reaction. Furthermore, the geometries of the initial complex and the product are also well reproduced by the ONIOM method. The calculated energy barrier at the B3LYP/6-31+G(d,p)//B3LYP/6-31G(d) level of theory is 8.6 kcal/mol, which is very similar to the ONIOM result. The spin-adduct product is exothermic by 12.5 kcal/mol, also similar to the ONIOM computational result (Table 4).

To gain insight as to whether *β*-CD facilitates trapping of HOO˙, four structures of initial complexes of HOO˙ and AMPO have been located as local minima (supporting

Table 3 Relative energies of the two isomers of 5*S*-*β*-CD-AMPO-HOO˙ (in kcal/mol)

	ONIOM(B3LYP/6-31G(d):PM3)	ONIOM(B3LYP/6-31+G(d,p):PM3)//ONIOM (B3LYP/6-31G(d):PM3)	B3LYP/6-31G(d)	B3LYP/6-31+G(d,p)//B3LYP/6-31G(d)
5*S*-*β*-CD-AMPO-HOO˙-1	0.0	0.0	0.0	0.0
5*S*-*β*-CD-AMPO-HOO˙-2	8.1	4.7	3.4	–0.1

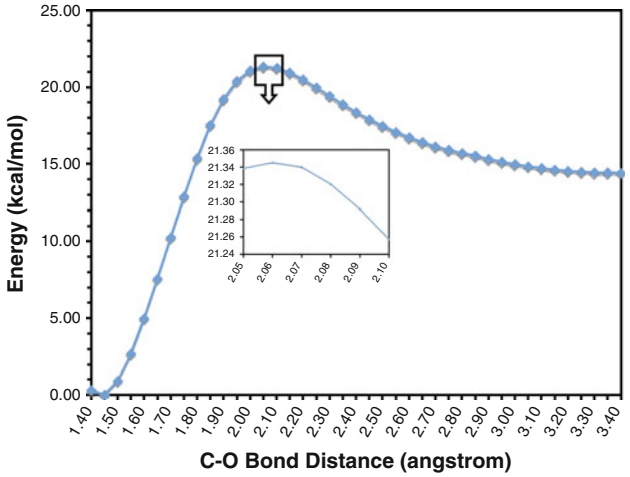

Fig. 4 Potential energy surface (PES) of the C_2–O_b bond cleavage of 5*R*-*β*-CD-AMPO-HOO˙. The C_2–O_b bond length (R) was stretched in steps of 0.05 Å, from 1.40 to 3.40 Å. At each value of R, the other coordinates of the complex were fully optimized. The summit of the PES was scanned in the units of 0.01 Å to obtain a more accurate peak on the PES

information, Figure S4). The transition states were then located for radical addition. Although the reaction barrier for the AMPO-(2*R*,5*S*)-2 conformer is very small, the high relative energy of the starting complex implies that this conformer may not play an important role in the reaction with HOO˙ (supporting information, Table S1). AMPO-(2*S*,5*S*)-1 conformer may play an important role in the reaction with HOO˙ due to the stability of the starting complex and the relatively low barrier for reaction. For the TS structure, the C···O distance is 2.10 Å that is very similar to the forming bond length for the *β*-CD-AMPO conjugate. The predicted energy barrier for HOO˙ trapping by AMPO is 9.1 kcal/mol, about 0.5 kcal/mol higher than the *β*-CD-AMPO energy barrier. It should be noted that the C···O distance in the starting complex of AMPO with HOO˙ is 3.89 Å, while the comparable distance for *β*-CD-AMPO with HOO˙ complex is only 3.47 Å. Comparing to the isolated AMPO model calculations, the role of the *β*-CD might be to anchor the HOO˙, which then makes the nitrone more accessible for radical addition.

3.3 5*R*-*β*-CD-A-$(CH_2)_n$-MPO (n = 1, 2, 3)

To optimize the reactivity of the *β*-CD-AMPO conjugate, a spacer unit with varying methylene units, $(CH_2)_n$ (n = 1, 2, 3), was evaluated between the AMPO segment and the *β*-CD moiety. The new molecules are presented by 5*R*-*β*-CD-A-$(CH_2)_n$-MPO (n = 1, 2, 3). For the nitrone, only the "internal" conformation was investigated based on the most stable "internal" *β*-CD-AMPO isomer. For the HOO˙ adduct, only the stable isomer for which the HOO group acts as a H-bond donor with *β*-CD was considered.

3.3.1 One methylene linker (n = 1)

The $N_7H_{7'}\cdots O_{1'}H_{1'}$ H-bond in 5*R*-*β*-CD-A-CH_2-MPO-HOO˙ is decreased by 0.21 Å compared with 5*R*-*β*-CD-A-MPO-

Table 4 Summary of the predicted kinetic barriers and thermochemistry for the HOO˙ attacking to 5R-*β*-CD-A-$(CH_2)_n$-MPO (n = 0, 1, 2, 3) (in kcal/mol)

	ONIOM(B3LYP/6-31G(d):PM3)	ONIOM(B3LYP/6-31+G(d,p):PM3)//ONIOM (B3LYP/6-31G(d):PM3)	B3LYP/6-31G(d)	B3LYP/6-31+G(d,p)//B3LYP/6-31G(d)
n = 0				
5*R*-*β*-CD-AMPO + HOO˙	0.0	0.0	0.0	0.0
TS	6.9	8.7	6.4	8.6
5*R*-*β*-CD-AMPO-HOO˙	–14.5	–12.4	–14.7	–12.5
n = 1				
5*R*-*β*-CD-A-CH_2-MPO + HOO˙	0.0	0.0	0.0	0.0
TS	5.3	6.2	5.1	6.2
5*R*-*β*-CD-A-CH_2-MPO-HOO˙	–15.5	–13.9	–14.9	–13.6
n = 2				
5*R*-*β*-CD-A-$(CH_2)_2$-MPO + HOO˙	0.0	0.0	–	–
TS	7.9	8.8	–	–
5*R*-*β*-CD-A-$(CH_2)_2$-MPO-HOO˙	–15.5	–13.8	–	–
n = 3				
5*R*-*β*-CD-A-$(CH_2)_3$-MPO + HOO˙	0.0	0.0	–	–
TS	8.8	9.4	–	–
5*R*-*β*-CD-A-$(CH_2)_3$-MPO-HOO˙	–14.4	–12.8	–	–

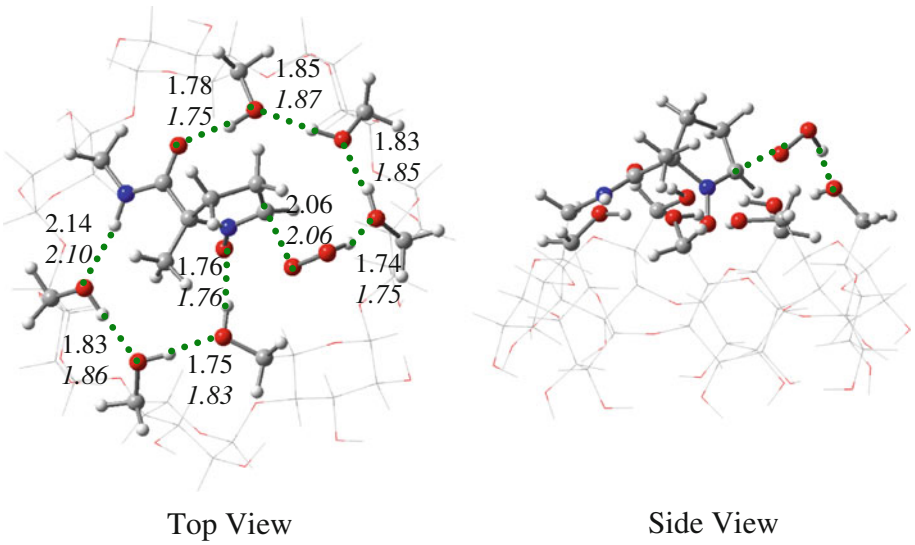

Fig. 5 Two views of the structure of the peak of potential energy surface (PES) of the C_2–O_b bond cleavage of 5*R*-*β*-CD-AMPO-HOO$^{\cdot}$ obtained at the ONIOM(B3LYP/6-31G(d):PM3) level. The bond lengths are shown in normal text. The bond lengths from the fully optimized TS structure of HOO$^{\cdot}$ addition to 5*R*-*β*-CD-AMPO obtained at the B3LYP/6-31G(d) level of theory are given in *italics* for comparison. The colors represent the following atoms: *gray* is for carbon, *white* is for hydrogen, *red* is for oxygen, and blue is for nitrogen. Bond lengths are shown in angstroms (Å)

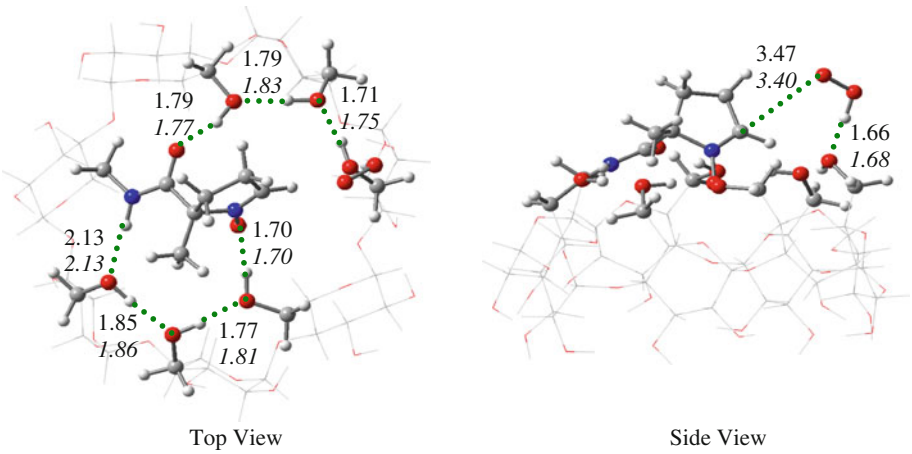

Fig. 6 Two views of the optimized structure of the starting complex of HOO$^{\cdot}$ with 5*R*-*β*-CD-AMPO obtained at the ONIOM(B3LYP/6-31G(d):PM3) level. The bond lengths are shown in normal text. The bond lengths from the fully optimized starting complex structure of HOO$^{\cdot}$ addition to 5*R*-*β*-CD-AMPO obtained at the B3LYP/6-31G(d) level of theory are given in italics for comparison. The *colors* represent the following atoms: *gray* is for carbon, *white* is for hydrogen, *red* is for oxygen, and blue is for nitrogen. Bond lengths are shown in angstroms (Å)

HOO$^{\cdot}$-1 (Fig. 7). The N_1–$O_1^{\cdot\cdot}H_{3'}O_{3'}$ H-bond is also shortened by 0.05 Å, suggesting that the H-bond might be strengthened and might help to protect the N_1–O_1 moiety of AMPO pointing into the cavity of *β*-CD.

The PES scan for the C_2–O_b bond length of 5*R*-*β*-CD-A-CH_2-MPO-HOO$^{\cdot}$ shows that the maximum occurs when the $C_2^{\cdot\cdot}O_b$ distance is 2.06 Å, very similar to that for the PES scan of 5*R*-*β*-CD-A-MPO-HOO$^{\cdot}$ (supporting information, Figures S5 and S6). As for the starting complex of 5*R*-*β*-CD-A-CH_2-MPO with HOO$^{\cdot}$, the $C_2^{\cdot\cdot}O_b$ distance is only 3.14 Å (supporting information, Figure S7). The HOO$^{\cdot}$ is more accessible to the addition site of the nitrone moiety in the starting complex. As a consequence, the predicted energy barrier to trap HOO$^{\cdot}$ is 6.2 kcal/mol for 5*R*-*β*-CD-A-CH_2-MPO using the ONIOM method, which is 2.5 kcal/mol lower than without a methylene linker as in 5*R*-*β*-CD-AMPO (Table 4). Moreover, the energy difference between reactant complex and product is 13.9 kcal/mol, which is 1.5 kcal/mol more exothermic than the 5*R*-*β*-CD-AMPO model (Table 4). The 5*R*-*β*-CD-A-CH_2-MPO is a much better agent to trap the HOO$^{\cdot}$ from both kinetic and thermodynamic points of view. The fully B3LYP optimized calculation of the addition of HOO$^{\cdot}$ to 5*R*-*β*-CD-A-CH_2-MPO was also performed. The TS structure and the starting complex have similar geometries to the ONIOM method. Moreover, the energy barrier predicted at the B3LYP/6-31G+(d,p)//B3LYP/6-31G(d) level of theory is also 6.2 kcal/mol.

3.3.2 Two methylene linkers (n = 2)

The H-bond chain in the optimized structure of 5*R*-*β*-CD-A-$(CH_2)_2$-MPO-HOO$^{\cdot}$ (supporting information, Figure S8)

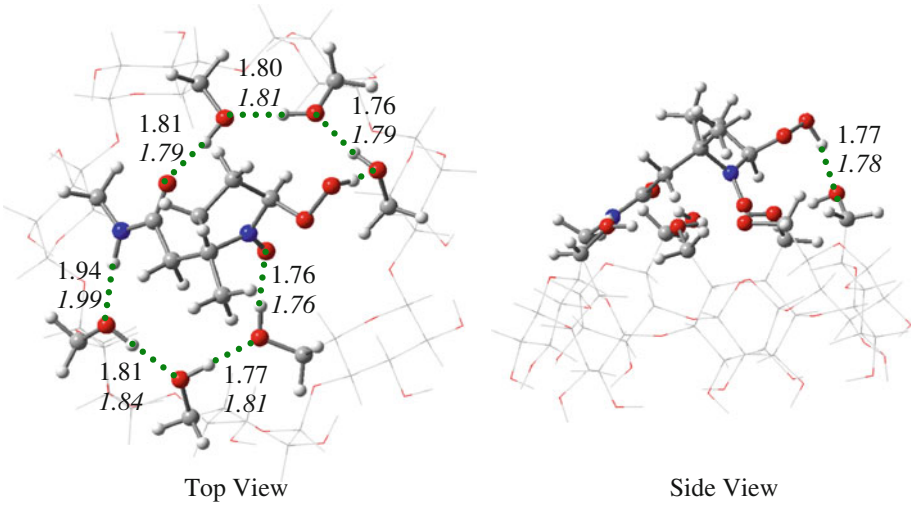

Fig. 7 Two views of the optimized structure of 5*R*-*β*-CD-A-CH_2-MPO-HOO$^{\cdot}$ obtained at the ONIOM(B3LYP/6-31G(d):PM3) level. The bond lengths are shown in normal text. The bond lengths from the fully optimized structure of 5*R*-*β*-CD-A-CH_2-MPO-HOO$^{\cdot}$ obtained at the B3LYP/6-31G(d) level of theory are given in italics for comparison. The *colors* represent the following atoms: *gray* is for carbon, *white* is for hydrogen, *red* is for oxygen, and *blue* is for nitrogen. Bond lengths are shown in angstroms (Å)

is very similar to 5*R*-*β*-CD-A-CH_2-MPO-HOO$^{\cdot}$ (the H-bond length differences are less than 0.05 Å). The PES scan for C_2–O_b bond cleavage of 5*R*-*β*-CD-A-$(CH_2)_2$-MPO-HOO$^{\cdot}$ indicates that the peak is achieved when the distance of $C_2^{\cdot\cdot}O_b$ reaches 2.06 Å (supporting information, Figures S9 and S10). The optimized initial complex (Figure S11) shows the distance between $C_2^{\cdot\cdot}O_b$ is 3.33 Å, approximately 0.19 Å longer than the corresponding distance in the initial 5*R*-*β*-CD-A-CH_2-MPO with HOO$^{\cdot}$ complex. The predicted ONIOM energy barrier for this two methylene linker model is 8.8 kcal/mol, which is 2.6 kcal/mol higher than the one methylene spacer (Table 4). It seems that the model with two methylene spacers is not the best choice.

3.3.3 Three methylene linkers (n = 3)

We also investigated three methylene spacers, but the characteristics of H-bond interactions change very little. The estimated reaction energy barrier is 9.4 kcal/mol for HOO$^{\cdot}$ addition to 5*R*-*β*-CD-A-$(CH_2)_3$-MPO based on the PES scan along the C_2–O_b coordinate (Table 4). Thus, it appears that one methylene spacer is the optimal linkage from a kinetic point of view.

4 Conclusions

AMPO ligated to *β*-CD by the amide group was computationally studied to gain insights on the effect of *β*-CD for spin-trapping properties of HOO$^{\cdot}$. For the nitrone, the "internal" conformation of 5*R*-*β*-CD-AMPO is preferred over the "external" conformation. When the hydroperoxyl radical addition product is formed, the most stable isomer has the N_1–O_1 moiety of AMPO pointing inside of the cavity of *β*-CD. This conformation might protect the nitroxyl (N_1–O_1) moiety of the spin-adduct product from oxidoreductants. The predicted energy barrier for HOO$^{\cdot}$ addition to the 5*R*-*β*-CD-AMPO is 8.7 kcal/mol, which is only marginally smaller than the AMPO nitrone itself. To investigate the length of the optimal 5*R*-*β*-CD-AMPO spacer, three different methylene, $(CH_2)_n$ ($n = 1, 2, 3$), systems were studied in which this linker was inserted between the amide and MPO. The structure with only one methylene spacer ($n = 1$) appears to be the best one due to the smallest energy barrier for hydroperoxyl radical addition. Moreover, 5*R*-*β*-CD-A-CH_2-MPO is also favored to trap HOO$^{\cdot}$ from a thermodynamic point of view.

Moreover, this study provided good calibration between the ONIOM(B3LYP:PM3) method and complete B3LYP calculations for systems involving cyclodextrins. Excellent agreement was observed in terms of energies and geometries. Compared with the very time-consuming B3LYP method for this system's size, the ONIOM method appears to offer significant advantage for the evaluation of the best 5*R*-*β*-CD-AMPO conjugate for trapping of radical species and to provide opportunities for the rational design of novel spin traps with improved properties [29].

Acknowledgments Financial support from the National Institutes of Health (R01-HL081248) is acknowledged. The Ohio Supercomputer Center (OSC) provided generous computational support of this research. We thank Dr. Shubham Vyas for technical assistance.

References

1. Halliwell B (2001) Drugs Aging 18:685
2. Zweier JL, Talukder MAH (2006) Cardiovasc Res 70:181
3. Zweier JL, Villamena FA (2003) Chemistry of free radicals in biological systems. In: Kukin ML, Fuster V (eds) Oxidative stress and cardiac failure. Futura Publishing Co., New York, p 67–95

4. De Grey ADNJ (2002) DNA Cell Biol 21:251
5. Halliwell B, Gutteridge JMC (1999) Free radicals in biology and medicine. Oxford University Press, Oxford
6. Lai EK, McCay PB, Noguchi T, Fong KL (1979) Biochem Pharm 28:2231
7. Shridhar R, Beaumont PC, Powers ELJ (1986) Radioanal Nuclear Chem 101:227
8. Kotake Y, Janzen EG (1991) J Am Chem Soc 113:9503
9. Janzen EG, Kotake Y, Hinton RD (1992) Free Rad Biol Med 12:169
10. Villamena FA, Zweier JL (2004) Antioxid Red Signal 6:619–629
11. Finkelstein E, Rosen GM, Rauckman EJ (1980) J Am Chem Soc 102:4994
12. Samuni A, Murali Krishna C, Riesz P, Finkelstein E, Russo A (1989) Free Rad Biol Med 6:141
13. Makino K, Hagiwara T, Imaishi H, Nishi M, Fuji S, Ohya H, Murakami A (1990) Free Radical Res Commun 9:233
14. Finkelstein E, Rosen GM, Rauckman EJ (1982) Mol Pharmacol 21:262
15. Buettner GR, Oberley LW (1978) Biochem Biophys Res Commun 83:69
16. Hinton RD, Janzen EGJ (1992) Org Chem 57:2646
17. Zeghdaoui A, Tuccio B, Finet J-P, Cerri V, Tordo P (1995) J Chem Soc, Perkin Trans 1:2087
18. Janzen EG, Zhang Y-K, Haire DL (1994) Magn Reson Chem 32:711
19. Fréjaville C, Karoui H, Tuccio B, Le Moigne F, Culcasi M, Pietri S, Lauricella R, Tordo P (1994) J Chem Soc Chem Commun 1793
20. Fréjaville C, Karoui H, Tuccio B, Le Moigne F, Culcasi M, Pietri S, Lauricella R, Tordo PJ (1995) Med Chem 38:258
21. Stolze K, Udilova N, Nohl H (2002) Biol Chem 383:813
22. Stolze K, Udilova N, Rosenau T, Hofinger A, Nohl H (2003) Biol Chem 384:493
23. Zhao H, Joseph J, Zhang H, Karoui H, Kalyanaraman B (2001) Free Radical Biol Med 31:599
24. Olive G, Mercier A, Le Moigne F, Rockenbauer A, Tordo P (2000) Free Radical Biol Med 28:403
25. Tsai P, Pou S, Straus R, Rosen GM (1999) J Chem Soc, Perkin Trans 2:1759
26. Rosen GM, Tsai P, Barth ED, Dorey G, Casara P, Spedding M, Halpern HJ (2000) J Org Chem 65:4460
27. Astolfi P, Marini M, Stipa P (2007) J Org Chem 72:8677
28. Ouari O, Polidori A, Pucci B, Tordo P, Chalier F (1999) J Org Chem 64:3554
29. Han Y, Liu Y, Rockenbauer A, Zweier JL, Durand G, Villamena FA (2009) J Org Chem 74:5369
30. Bardelang D, Rockenbauer A, Karoui H, Finet JP, Tordo P (2005) J Phys Chem B 109:10521
31. Bardelang D, Charles L, Finet JP, Jicsinszky L, Karoui H, Marque SRA, Monnier V, Rockenbauer A, Rosas R, Tordo P (2007) Chem Eur J 13:9344
32. Polovyanenko DN, Marque SRA, Lambert S, Jicsinszky L, Plyusnin VF, Bagryanskaya EG (2008) J Phys Chem B 112:13157
33. Han Y, Tuccio B, Lauricella R, Villamena FA (2008) J Org Chem 73:7108
34. Villamena FA, Merle JK, Hadad CM, Zweier JL (2007) J Phys Chem A 111:9995
35. Villamena FA, Hadad CM, Zweier JL (2003) J Phys Chem A 107:4407
36. Villamena FA, Hadad CM, Zweier JL (2004) J Am Chem Soc 126:1816
37. Villamena FA, Hadad CM, Zweier JL (2005) J Phys Chem A 109:1662
38. Villamena FA, Merle JK, Hadad CM, Zweier JL (2005) J Phys Chem A 109:6083
39. Villamena FA, Merle JK, Hadad CM, Zweier JL (2005) J Phys Chem A 109:6089
40. Villamena FA, Rockenbauer A, Gallucci J, Velayutham M, Hadad CM, Zweier JL (2004) J Org Chem 69:7994
41. Svensson M, Humbel S, Froese RDJ, Matsubara T, Sieber S, Morokuma K (1996) J Phys Chem 100:19357
42. Vreven T, Byun KS, Komaromi I, Dapprich S, Montgomery JA Jr, Morokuma K, Frisch MJ (2006) J Chem Theory Comput 2:815
43. Frisch MJ, Trucks GW, Schlegel HB, Scuseria GE, Robb MA, Cheeseman JR, Montgomery JA Jr, Vreven T, Kudin KN, Burant JC, Millam JM, Iyengar SS, Tomasi J, Barone V, Mennucci B, Cossi M, Scalmani G, Rega N, Petersson GA, Nakatsuji H, Hada M, Ehara M, Toyota K, Fukuda R, Hasegawa J, Ishida M, Nakajima T, Honda Y, Kitao O, Nakai H, Klene M, Li X, Knox JE, Hratchian HP, Cross JB, Bakken V, Adamo C, Jaramillo J, Gomperts R, Stratmann RE, Yazyev O, Austin AJ, Cammi R, Pomelli C, Ochterski JW, Ayala PY, Morokuma K, Voth GA, Salvador P, Dannenberg, JJ, Zakrzewski VG, Dapprich S, Daniels AD, Strain MC, Farkas O, Malick DK, Rabuck AD, Raghavachari K, Foresman JB, Ortiz JV, Cui Q, Baboul AG, Clifford S, Cioslowski J, Stefanov BB, Liu G, Liashenko A, Piskorz P, Komaromi I, Martin RL, Fox DJ, Keith T, Al-Laham MA, Peng CY, Nanayakkara A, Challacombe M, Gill PMW, Johnson B, Chen W, Wong MW, Gonzalez C, Pople JA (2004) Gaussian 03, revision B.05. Gaussian, Inc., Wallingford CT
44. Becke AD (1993) J Chem Phys 98:5648
45. Lee C, Yang W, Parr RG (1988) Phys Rev B 37:785
46. Stewart JJP (1989) J Comput Chem 10:221
47. Liu L, Guo QX (2004) J Incl Phenom Macrocycl Chem 50:95
48. Gordon MT, Lowary TL, Hadad CM (2000) J Org Chem 65:4954
49. Anconi CPA, Nascimento CS, Fedoce-Lopes J, Dos Santos HF, De Almeida WB (2007) J Phys Chem A 111:12127